

Arbitrary Axis Rotating Surface Acoustic Wave Micro Motor

Ricky T. Tjeung, Mark S. Hughes, Leslie Y. Yeo, and James R. Friend*

Micro/Nanophysics Research Laboratory, Monash University, Clayton 3800, Victoria, Australia

* E-mail: James.Friend@monash.edu

Abstract- We present a surface acoustic wave (SAW) actuated rotating micro motor. The rotors are 1 millimeter metal spheres which are placed on the surface of a Lead Zirconate Titanate (PZT) substrate with IDTs designed to generate SAW with $\sim 700 \mu\text{m}$ wavelength. A Laser Doppler Vibrometer (LDV) was used to visualize the travelling SAW and the result was compared with the rotation of the rotor. The motor transient responses are presented, along with its torque-speed curve. The maximum rotational speed and torque reported were ~ 1000 rpm and $\sim 14 \mu\text{N}\cdot\text{mm}$, respectively. Arbitrary motions have also been demonstrated utilizing a magnetic pre-load and multiple IDTs activation.

Keywords: rotational micro motor, surface acoustic wave, ultrasonics motor, piezoelectric

I. BACKGROUND

A surface acoustic wave (SAW) motor is a millimeter size motor actuated by travelling waves. Most applications utilize the Rayleigh wave, a type of acoustic wave which is confined to travel along the surface of a piezoelectric material [1-8].

Work on developing various linear SAW micro motors have been performed by Kurosawa et al [1-3] and Xing et al [4]. The systems consist of a rotor preloaded with magnet, set to linearly move along a slider. The maximum speed and force achieved were 0.9 m/s and 18 N respectively for a 125 V_p input voltage [3].

We present another type of SAW micro motor. Utilizing a metal sphere as the rotor, we developed a rotating micro motor, instead of a linear motor. The substrate material selected for this purpose was lead zirconate titanate (PZT) rather than the more common 127.68° Y-X cut Lithium Niobate (LiNbO₃) due to the

anisotropic nature of the material. Using PZT as the piezoelectric substrate, arbitrary rotating motion can be achieved.

II. CURRENT RESULT

SAWs were generated by applying a continuous sinusoidal electrical input into an interdigital transducer (IDT, Ag 7-finger pair electrode) patterned on a surface of the PZT ceramic substrate. The devices were designed to work with a 3.2 MHz resonance frequency, which results in a 700 μm wavelength.

Fig. 1 and 2 show the configuration of the rotating micro motor. A metal sphere (1 mm diameter) as the rotor was placed onto a blind hole drilled on the PZT surface. A permanent magnet, with strength of $0.088 \pm 0.002\text{T}$ was used as the pre-load. The blind hole (0.25 mm) was used to confine the rotor from translating during operation.

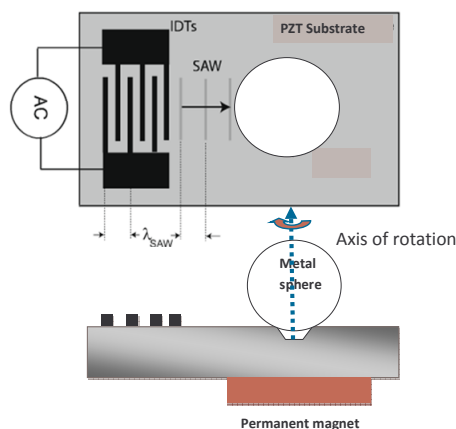
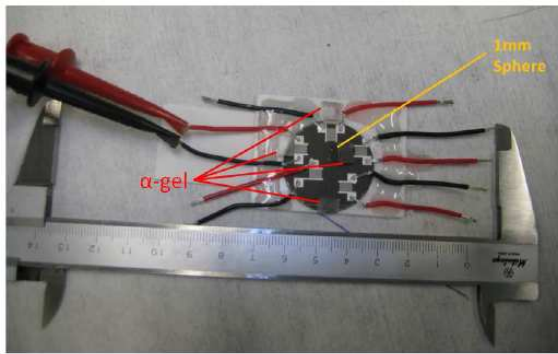
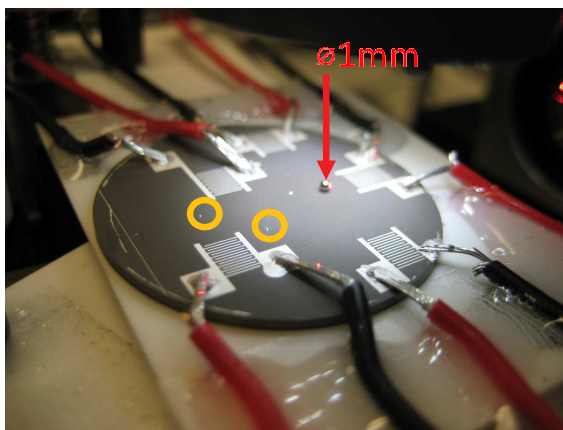


Fig. 1. Schematic representation of the rotating micro motor.



(a)



(b)

Fig. 2. The arbitrary axis SAW micro motor with 1mm diameter steel rotor on PZT substrate with 3.2MHz IDTs. An Alpha GEL (Taica Corporation, Japan) is used to absorb reflected SAWs from substrate boundaries, mitigating standing waves; (b) the yellow circles indicate the blind holes.

Visualization of the travelling SAW along the PZT surface with the hole was done using a Laser Doppler Vibrometer (LDV; Polytec PI MSA-400, Waldbrunn, Germany). The result is presented as fig.3. It was also observed that the SAW continues to travel along the blind hole.

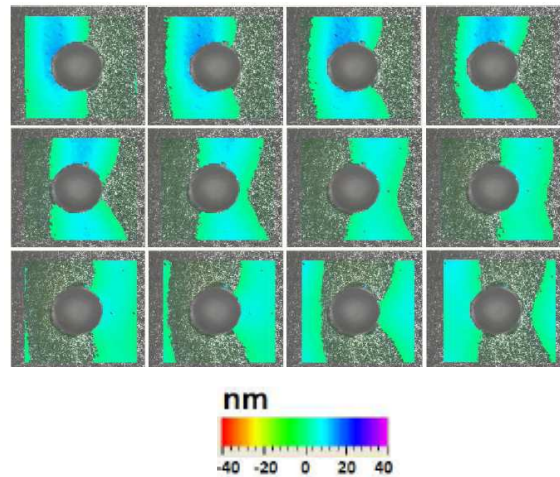


Fig. 3. Consecutive images of Laser Doppler Vibrometer data of a 700 μm SAW travelling along a 250 μm blind hole in PZT. The propagation direction of the SAW is from left to right.

After the completion of the SAW visualization, the next step was to characterize the performances of the motor during operation. Hypothesis formed after the LDV result analysis shows that the rotor should rotate with axis of rotation parallel to the surface and perpendicular to the SAW propagation path; experimental results prove this hypothesis closely. The schematic of this operation can be viewed in fig. 4.

Further experiments showed that the axis of rotation can be altered by introduction of a pre-load. The axis of rotation with magnetic pre-load is normal to the surface of the substrate. Fig. 5 shows the two modes of operation (with and without pre-load).

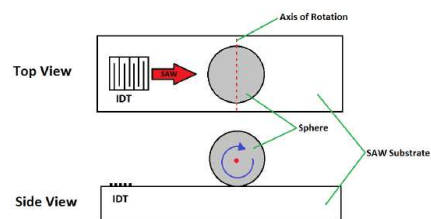


Fig. 4. Schematic illustration of one mode of operation, i.e. without any pre-load. The blue arrow shows the rotor rotation direction, the axis of rotation is perpendicular to the SAW propagation path.

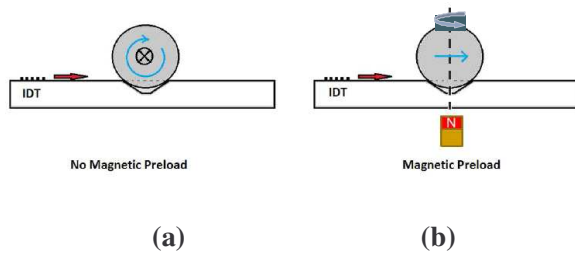


Fig. 5. Schematic illustrations of two modes of operation. The blue arrow shows the rotor rotation directions. The axis of rotation can be altered with introduction of a magnetic pre-load ($0.088 \pm 0.002T$) from (a) perpendicular to the SAW propagation path to (b) normal to the substrates surface. This could be used as a mechanism to achieve the arbitrary axis rotation.

Successive images of the rotor rotation during operation are shown in fig. 6. The images were captured using a high speed camera (Motion BLITZ, Mikroton GMBH) at 1000 frames per seconds. The operation was with pre-load hence the normal axis of rotation.

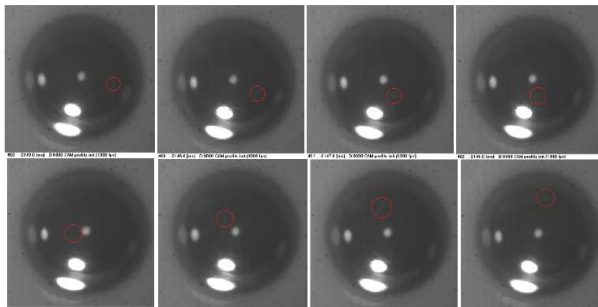


Fig. 6. Successive images of the motor during one mode of operation. The motor was running with the magnetic pre-load, hence the axis of rotation is normal to the substrates surface. The images were captured using a high speed camera (Motion BLITZ, Mikroton GMBH) at 1000 frames per seconds.

The motor start-up speeds were measured using a Laser Tachometer (Canon, S-100Z). Input power was provided using a signal generator (NF Wave Factory, WF1946 2CH) coupled with an amplifier (NF High Speed Bipolar Amplifier, HSA 4101). The transient response is shown in fig. 7. The torque is calculated using the method proposed by Nakamura et al [5] and shown in fig. 8.

Using single IDT activations, the rotor rotates with axis of rotation normal to the surface of the substrate. With the $250 \mu m$ blind hole configurations and

maximum input power of $65 V_p$, the maximum rotation speed and torque achieved were ~ 1000 rpm and $\sim 14 \mu N \cdot mm$ respectively. The micro motor was able to operate without performance degradation up to 30 sec.

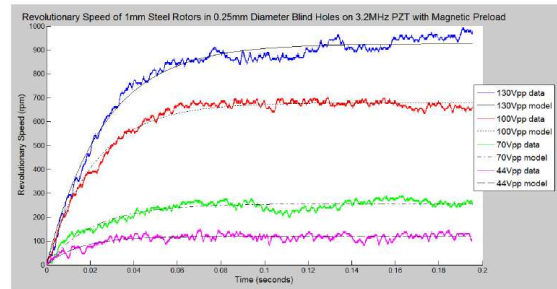


Fig. 7. The transient response of the motor during operation with the magnetic pre-load. The motor start-up speeds were measured using a Laser Tachometer (Canon, S-100Z). The maximum speed achieved was approximately 1000 rpm.

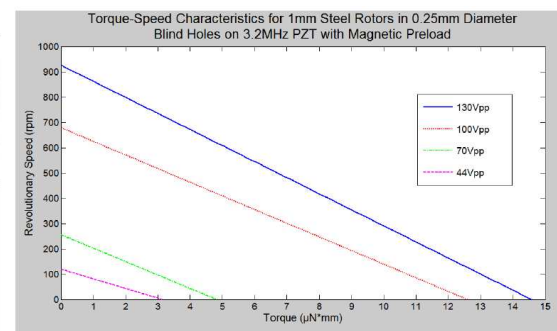


Fig. 8. The torque speed characteristic of the motor during operation with the magnetic pre-load. The torque was calculated using the method proposed by Nakamura et al [5]. The maximum torque achieved was over $14 \mu N \cdot mm$.

We subsequently continued to visualize the SAW actuated by multiple IDTs activation. These are also essential for achieving arbitrary motions. The results can be viewed on fig. 9. The measured area is located in front of two IDTs, whose axes of wave propagation are perpendicular to each other. We followed by demonstrating the rotor capability to rotate in arbitrary directions. The rotational directions of the rotor follow the LDV results closely.

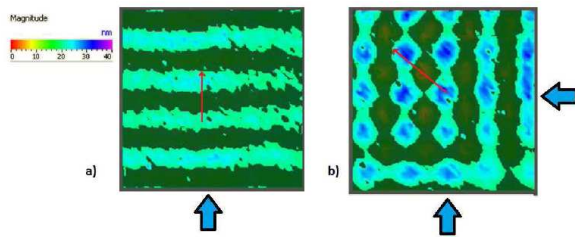


Fig. 9. Laser Doppler Vibrometer (LDV) visualization of SAW generated by multiple IDTs actuations. Fig. 9 (a) illustrates the SAW propagation from one IDT (below the image), while fig. 9 (b) illustrates the SAW propagation at the intersection from two perpendicularly orientated IDTs. The SAW travelling directions are indicated by the blue arrows and the motion of the peak displacements are indicated by the inset red arrows.

ACKNOWLEDGMENT

Funding provided for this study by the Australian DPMC, ARC and NHMRC are gratefully acknowledged.

REFERENCES

- [1] M. K. Kurosawa, M. Chiba, and T. Higuchi, "Evaluation of a surface acoustic wave motor with a multi-contact-point slider," *Smart Mater. Struc.*, pp. 305-311, 1998.
- [2] K. Asai and M. K. Kurosawa, "Performance Estimation of Surface Acoustic Wave Motor Using Simulation Model of Friction Drive," *Electronics and Communications in Japan, Part3. Vol. 88, No. 1*, 2005.
- [3] K. Sakano, M. K. Kurosawa, and T. Shigematsu, "Driving Characteristic of a Surface Acoustic Wave Motor using a Flat-Plate Slider," *Advanced Robotics* 24, pp. 1407-1421, 2010.
- [4] Y. Xing, Y. Li, J. Zhang, and G. Gao, "Surface Acoustic Wave Linear Motor for Two-dimensional Optical Positioning System," *Proceedings of the 2009 4th IEEE International Conference on Nano/Micro Engineered and Molecular Systems*, January 2009.
- [5] K. Nakamura, M. Kurosawa, H. Kurebayashi, and S. Ueha, "An Estimation of Load Characteristics of an Ultrasonics Motor by Measuring Transient Responses" *IEEE Transactions on Ultrasonics, Ferroelectrics, and Frequency Control*, Vol. 38, No. 5, September 1991.
- [6] M. Kurosawa, M. Takahashi, and T. Higuchi, "Friction Drive Surface Acoustic Wave Motor," *Ultrasonics*, 34, pp. 243-246, 1996.
- [7] M. K. Kurosawa, "State-of-the-art Surface Acoustic Wave Linear Motor and Its Future Applications," *Ultrasonics*, 38, pp. 15-19, 2000.
- [8] M. Takahashi, M. Kurosawa, and T. Higuchi, "Optimum Contact Conditions for Miniaturized Surface Acoustic Wave Linear Motor" *Ultrasonics*, 38, pp. 51-53, 2000.